www.MaterialsViews.com

ADVANCED
FUNCTIONAL
MATERIALS
www.afm-journal.de

FULL PAPER

n-GaAs/InGaP/p-GaAs Core-Multishell Nanowire Diodes for Efficient Light-to-Current Conversion

Christoph Gutsche,* Andrey Lysov, Daniel Braam, Ingo Regolin, Gregor Keller, Zi-An Li, Martin Geller, Marina Spasova, Werner Prost, and Franz-Josef Tegude

Heterostructure n-GaAs/InGaP/p-GaAs core-multishell nanowire diodes are synthesized by metal-organic vapor-phase epitaxy. This structure allows a reproducible, selective wet etching of the individual shells and therefore a simplified contacting of single nanowire p-i-n junctions. Nanowire diodes show leakage currents in a low pA range and at a high rectification ratio of 3500 (at ±1V). Pronounced electroluminescence at 1.4 eV is measured at room temperature and gives evidence of the device quality. Photocurrent generation is demonstrated at the complete area of the nanowire p-i-n junction by scanning photocurrent microscopy. A solar-conversion efficiency of 4.7%, an open-circuit voltage of 0.5 V and a fill factor of 52% are obtained under AM 1.5G conditions. These results will guide the development of nanowire-based photonic and photovoltaic devices.

1. Introduction

As recently highlighted, the field of semiconductor nanowires has become one of the most-active research areas within nano-scale science during the past decade.[1] For photonic applications, GaAs-based direct-bandgap materials are primarily important. The significance of shell or multiple-shell structures for the functionality of nanowire-based optoelectronic devices was described a few years ago by Lauhon et al.,[2] followed by various reports and investigations on this topic.[3–5] As one benefit, the surface of the nanowire core can be passivated by a wide-bandgap semiconductor shell. This significantly increases the lifetime of minority carriers in the core and improves the optical performance of nanowire devices.[6,7] In addition a shell with a lower refractive index can promote waveguiding in the nanowire core,[6] as proven by coaxial GaAs/GaAsP[8] and InGaAs/GaAs[9] nanowire lasers. Moreover, the growth temperatures typically used for nanowire-shell growth are similar to those of conventional layer epitaxy

(600–700 °C) and are thus favorable for the decomposition of precursors. Light-emitting diodes (LEDs) based on heterostructured GaAs/InGaP core-shell,[10] GaAs/AlGaAs core-multishell,[11] and GaAs-based core-multishell[12] nanowires have been demonstrated. Compared with thin-film devices, nanowire-based solar cells[13] hold the promise of reducing reflection losses[14,15] for incident sunlight and improving light collection.[16] Nanowires may be grown at a very-high growth rate on various cheap,[17] flexible and low-weight substrates, aiming for economically competitive low-weight applications. Using direct-bandgap-semiconductor nanowires, an ultra-short absorption length can be implemented enabling the use of coaxial core-shell-type devices. The core-shell geometry provides an orthogonalization of the charge and light pathways. It has been predicted that this approach will yield an extremely efficient carrier collection.[18]

The photovoltaic properties of molecular-beam-epitaxy (MBE)-grown GaAs p-i-n[11] and p-n radial structures[12] have been investigated by means of photocurrent measurements, resulting in conversion efficiencies of 4.5%[19] and 0.83%,[20] respectively. In contrast to MBE, metal-organic vapor-phase epitaxy (MOVPE) is the primary industrial growth technique, providing a uniform, large-area deposition, which is desirable for mass production. Recently, solar cells consisting of dense arrays of radial GaAs nanopillar p-n junctions grown via selective-area MOVPE have been demonstrated with a conversion efficiency of 2.54%.[21]

In this work we report on the growth, fabrication and opto-electronic characterization of n-GaAs/InGaP/p-GaAs hetero-structure core-multishell nanowire diodes, grown via the vapor-liquid-solid (VLS) growth mode in MOVPE. In the first part, we investigate a doping effect in the GaAs nanowire shell using a carbontetrabromide (CBr_4) doping precursor. In the second part of the manuscript, selective etching of the different shells and the structural characterization of the fabricated single p-i-n nanowire diodes are described. Finally we present the optoelectronic performance of the fabricated nanowire p-i-n junctions, investigated by electroluminescence, scanning photocurrent microscopy and power-dependent photocurrent measurements, as well as by direct current (DC) characterization under standard illumination. In addition, the role of the intermediate InGaP shell is discussed.

C. Gutsche, A. Lysov, Dr. I. Regolin, G. Keller, Prof. F.-J. Tegude
Department of Solid-State Electronics and CeNIDE University of Duisburg-Essen
Lotharstr. 55, ZHO, D-47057 Duisburg, Germany
E-mail: christoph.gutsche@uni-due.de
D. Braam, Dr. Z.-A. Li, Dr. M. Geller, Dr. M. Spasova
Department of Experimental Physics and CeNIDE
University of Duisburg-Essen
Lotharstr. 1, D-47057 Duisburg, Germany
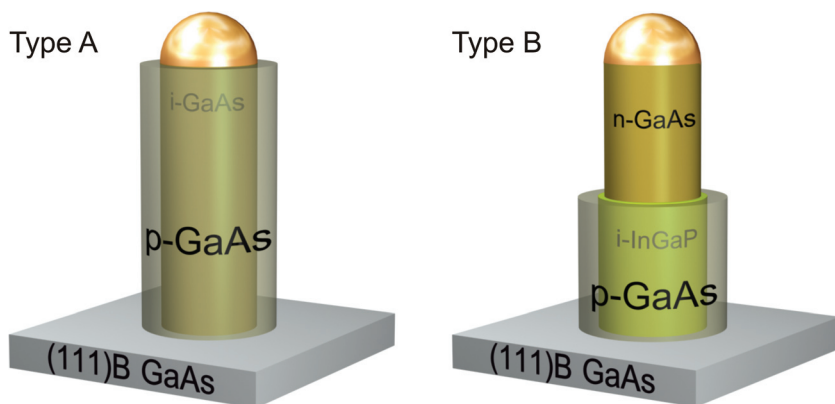
Figure 1. Growth schematics of the two investigated structures: **Type A**: i-GaAs/p-GaAs core-shell nanowires; **Type B**: n-GaAs/InGaP/p-GaAs core-multishell nanowires.

2. Results and Discussion

Two different types of GaAs-based core-shell and core-multi-shell nanowires were investigated in this study. The first type of nanowires consisted of a non-intentionally doped (nid) GaAs nanowire core with a p-GaAs shell wrapped around it (subsequently denoted as **Type A**). The coaxial nanowire pin-diodes consisted of an n-GaAs core surrounded by lattice-matched nid-InGaP and a p-GaAs shell (subsequently denoted as **Type B**). Schematic drawings of both these studied nanowire types are shown in **Figure 1**.

2.1. Electrical Characterization of the p-GaAs Shell

In the first set of experiments, we investigated a possible doping effect, using CBr_4 as a doping precursor during the

GaAs shell growth on the **Type-A** nanowire samples. **Figure 2**a shows representative transfer (black color, bottom x- and left y-axis) and drain-source $I-V$ characteristics (grey color, upper x- and right y-axis) of fabricated i-GaAs/p-GaAs core-shell top-gated metal–insulator-semiconductor field-effect-transistor (MISFET) structures. The corresponding $I-V$ characteristics measured without applied gate bias ($V_{GS} = 0$ V) were perfectly ohmic, exhibiting a high current of 20 μA at $V_{DS} = 1$ V. Since the parallel current flow through the i-GaAs nanowire core was located in the low-pA range,[22] the measured current could be assigned completely to the outer p-GaAs shell. The use of CBr_4 implies a p-type conductivity, which was verified by the depicted transfer characteristics. As the channel conductance increased with negative gate bias, this experiment proved the p-type doping effect using CBr_4. In contrast to the alternative p-dopant, zinc, carbon has the advantage of being less diffusive,[23] which results in the possibility of achieving high doping levels and abrupt doping profiles.[24] Therefore CBr_4 is perfectly suited to the p-type doping of vapor-solid (VS)-grown GaAs-based nanowire shells.

In order to estimate the carrier concentration in the p-GaAs shell, we analyzed the electrical conductivity of a number of i-GaAs/p-GaAs core-shell nanowires using the transport model described in detail previously.[22] This model was adopted by subtraction of the undoped GaAs-core radius r_{i-GaAs} from the total nanowire radius r_0. The i-GaAs-core radius was fixed here to $r_{i-GaAs} = 50$ nm, corresponding to the radius of the Au seed particles. Hence, the nanowire resistance was estimated as follows:
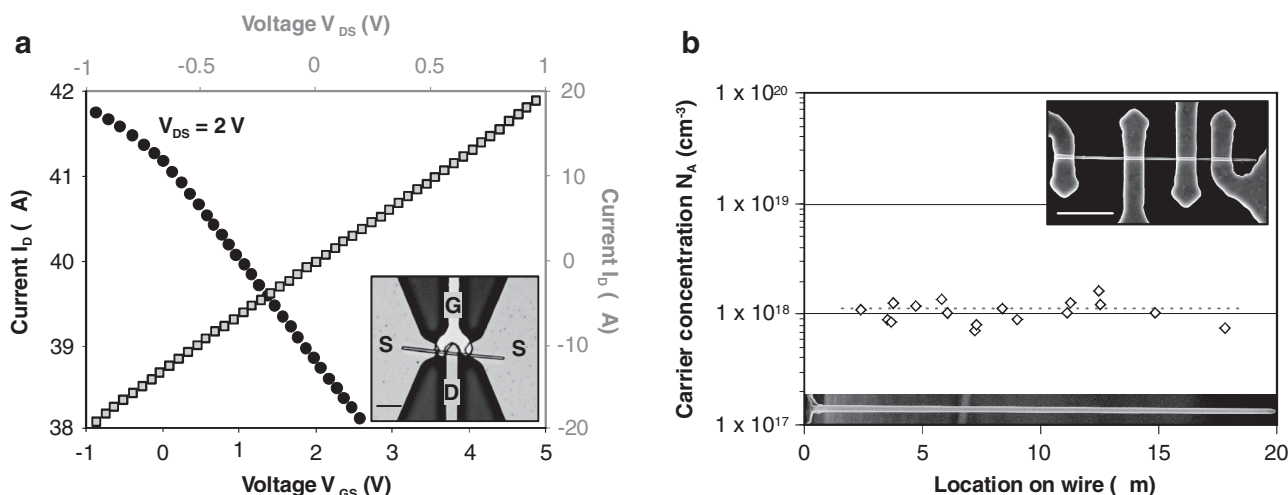
Figure 2. a) Transfer (black color, bottom x- and left y-axis) and drain-source $I-V$ characteristics (grey color, upper x- and right y-axis) of fabricated i-GaAs/p-GaAs core-shell MISFET, proving the ohmic character (grey) and, additionally, the p-type behavior (black). The inset shows an optical micrograph (scale bar is 5 μm): left and right: source contact pads; bottom: drain contact; top: two-finger top-gate; the nearly horizontal stripe is the nanowire. b) p-GaAs-shell carrier concentrations determined at different positions of the various wires. The dotted line indicates the mean value of $N_A = 1.1 \times 10^{18}$ cm^{-3}. A length of zero represents the wire bottom, as also indicated by the lower SEM inset. The upper-right inset exemplarily shows one characterized i-GaAs/p-GaAs core-shell nanowire device with four contacts (scale bar is 5 μm).

www.MaterialsViews.com

ADVANCED
FUNCTIONAL
MATERIALS
www.afm-journal.de

FULL PAPER

$$R = \frac{1}{q \cdot N_A \cdot \mu(N_A)} \cdot \frac{l}{\pi \cdot (r_0 - d_{spc})^2 - \pi \cdot (r_{i-GaAs})^2} \tag{1}$$

In Equation 1, N_A, is the carrier concentration, μ is the hole mobility and d_{spc} is the surface-depletion width. The geometrical data of the nanowires, such as the segment l and the complete core-shell-nanowire radius r_0, were determined by means of scanning electron microscopy (SEM). The assumed dependence of the hole mobility μ and depletion width d_{spc} on the dopant density N_A is described elsewhere.[22] In this way, the wire resistance R is correlated to the shell acceptor concentration only. We used transmission-line-measurement (TLM) structures with four contacts on different positions along the wire (see inset of Figure 2b), leading to a statistical evaluation. In Figure 2b, the corresponding carrier concentrations are depicted against the location on the wire. It is evident that the data show a small spreading, with a mean carrier concentration of $N_A = 1.1 \times 10^{18}$ cm^{-3}, indicated by the dotted line. Therefore, carbon incorporation during VS growth was homogeneous along the nanowire length.

2.2. Morphology and Selective Etching of n-GaAs/InGaP/p-GaAs

After the successful p-GaAs-shell doping, we focused on the characterization of the synthesized n-GaAs/InGaP/p-GaAs core-multishell nanowires (**Type-B** samples). **Figure 3**a shows an SEM micrograph of the as-grown structure, where the image in the inset was taken on the base of a transferred nanowire to obtain a cross-sectional view. The nanowire core appears to have a dodecagonal shape with a mixture of {110} and {112}

side facets (for detailed information, see the Supporting Information). After growth of the InGaP shell at higher temperature, a translation into pure {110} side facets was observable, which remained for the outer p-GaAs shell. A similar phenomenon has been reported for GaAs/InAlAs core-shell nanowires,[25] as well as for GaP/GaAs core-multishell nanowires,[26] and its formation mechanisms have been discussed.[25]

The selective etching of the different shells (**Type B**) was arranged in five main steps. Firstly, a special photoresist (AR-P 5320) was spin-coated onto the as-grown samples. The photoresist from the upper part of the wires was removed by a short dip in the appropriate developer (AR 300-26), ensuring that approximately half of the core-multishell nanowires were still embedded. Afterwards, the outer p-GaAs shell was etched in diluted phosphoric acid (H_3PO_4:H_2O_2:H_2O in a ratio of 1:1:25), which is known to stop at the InGaP material.[27] Next, the exposed InGaP shell was removed using diluted hydrochloric acid (HCL:H_2O in a ratio of 3:1), which allows selective etching of InGaP over GaAs.[28] Hence the inner, VLS-grown n-GaAs-nanowire core was not affected, independent of a possibly over-valued etch time. The protecting photoresist was subsequently removed from the readily etched samples by soaking in hot acetone and propanol. Material-selective etching allowed inhomogenities in the shell thickness of individual nanowires to be compensated and ensured a robust fabrication process.

The SEM micrograph depicted in Figure 3b shows a core-multishell nanowire after selective etching of the outer shells. It is evident that the upper half of the nanowire exhibits a smaller diameter of approximately 100 nm, which matches the diameter of the n-type GaAs core. A direct proof for the successful removal of the two outer shells by the etching process was
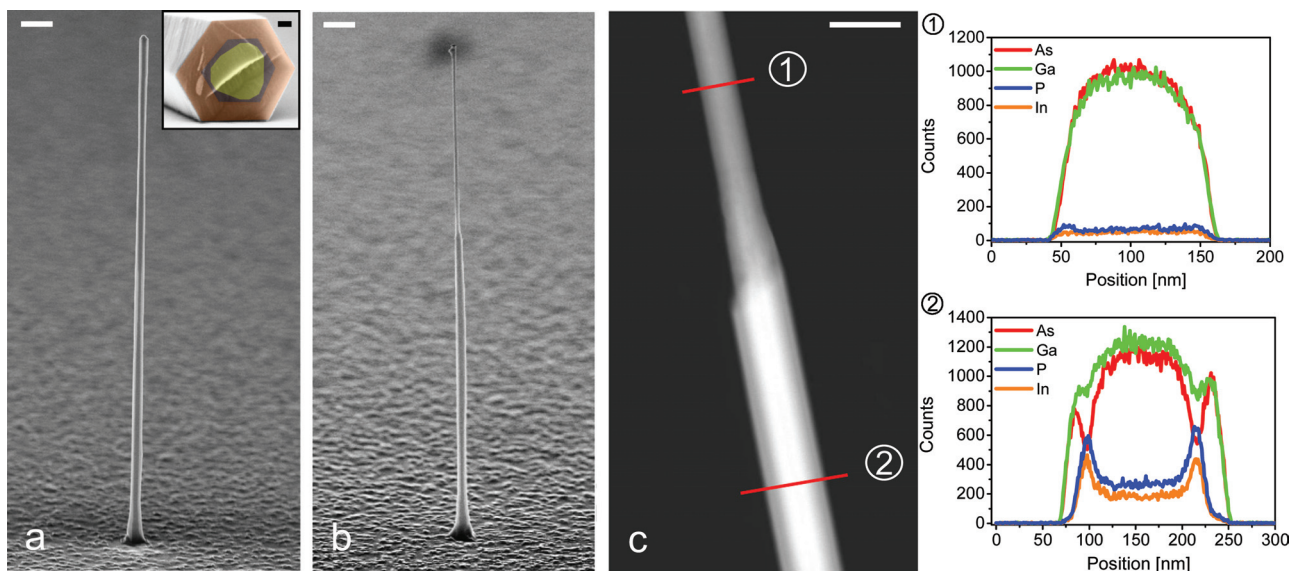
Figure 3. a) SEM microscopy image of the as-grown n-GaAs/InGaP/p-GaAs core-multishell structure (scale bar is 1 μm). The image in the inset (scale bar = 30 nm) was taken on the base of a transferred nanowire to obtain a cross-sectional view. Colors have been superimposed to visualize the different parts. It is evident that the dodecagonal shape of the nanowire core, with a mixture of {110} and {112} side facets, translates into pure {110} side facets for the outer shells grown at higher temperatures (for detailed information, see Supporting Information). b) A core-multishell nanowire diode after halfway selective etching of the outer shells (scale bar is 1 μm). c) TEM image of the transition between the etched (1) and unetched (2) region (scale bar is 200 nm). The corresponding EDS linescans clearly verify the GaAs core (1) and the GaAs/InGaP/GaAs core-multishell structure (2). Please note that the nanowire in Figure 3 c has a decreased shell thickness compared with the p-i-n diodes investigated subsequently.
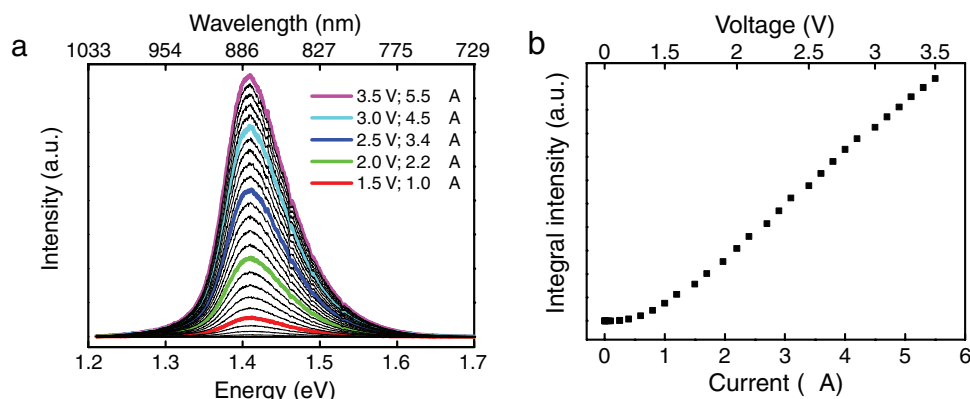
Figure 4. a) EL spectra for several bias/current conditions at room temperature. The thin black curves indicate intermediate values. b) Linear plot of the EL intensity as a function of the injected current. The upper *x*-axis shows the corresponding bias.

given by line-scan energy-dispersive X-ray spectroscopy (EDS) measurements in a transmission electron microscope (TEM), as shown in Figure 3c. The elemental profiles extracted from the line-scan EDS measurements clearly show that the unetched part was composed of GaAs/InGaP/GaAs core-multishells and the etched part was composed of GaAs. Note that, in the etched part, the P and In are plotted in the elemental profile just for comparison, though their compositions were less than 2 at%. Hence, the etching procedure enabled selective contacting of the n-GaAs nanowire core, as well as of the p-GaAs nanowire shell, and therefore enabled a further optoelectrical characterization of the realized p-i-n core-multishell nanowire diode.

2.3. Optoelectrical Characterization of the Fabricated n-GaAs/InGaP/p-GaAs Diodes

To characterize the optoelectrical performance of the fabricated nanowire diodes, a set of electrical, electroluminescent and photovoltaic measurements was carried out on the same nanowire device. This contacted core-multishell nanowire diode had a total diameter of 317 nm, which comprised the n-GaAs core ($r_{n\text{-GaAs}} \approx 50$ nm) and the surrounding InGaP ($r_{InGaP} \approx 20$ nm) and p-GaAs ($r_{p\text{-GaAs}} \approx 90$ nm) shells. The emitted light was measured at room temperature. **Figure 4**a shows the typical electroluminescence (EL) spectra for several bias/current conditions. The EL peak position is at around 1.42 eV, which is in good agreement with the GaAs bandgap at room temperature ($E_g = 1.42$ eV). According to the band diagram (see also **Figure 5** for the unbiased case), a recombination of carriers in the n-GaAs nanowire core is unlikely. Due to the intermediate InGaP shell, the significant potential barrier in the valence band prevents the injection of holes from the p-GaAs shell. Therefore, it is reasonable to assume that, in LED operation, electrons from the n-GaAs core are injected into the p-GaAs shell where recombination takes place. Above a threshold current of 0.5 μA, the EL intensity increased linearly with current injection up to 6 μA (Figure 4b). The existence of pronounced EL at room temperature constitutes the optical quality of the fabricated p-i-n diode.
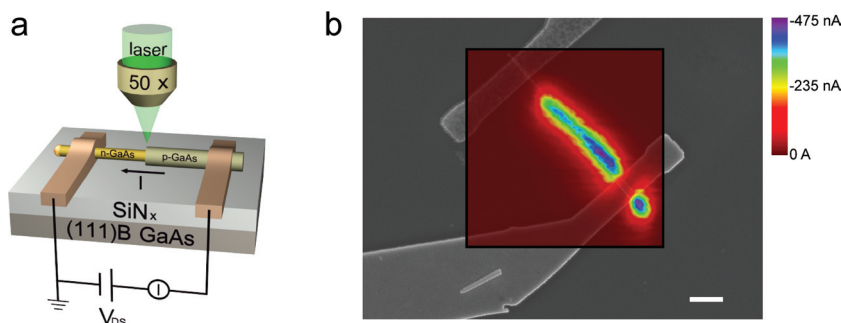
A cut-out, 1D band-diagram section for the material sequence of the fabricated device is proposed in Figure 5, having used a
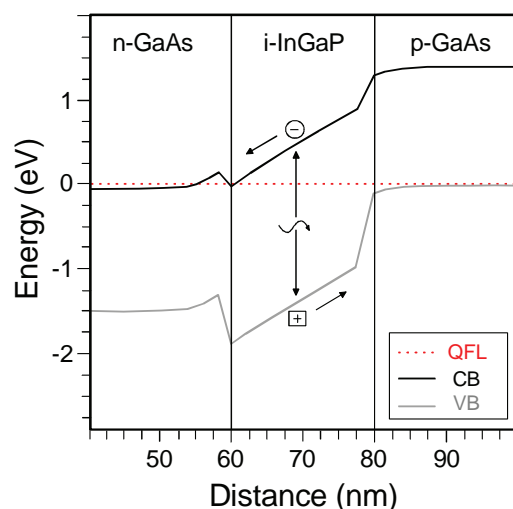
Figure 5. Cut-out, 1D band-diagram section for the material sequence of the fabricated device, calculated using a Poisson solver in a Silvaco simulation tool. The diagram was calculated for the unbiased case, while the materials and dopings were as follows: n-GaAs core, $N_D = 4 \times 10^{18}$ cm^{-3}; i-InGaP shell, nid; p-GaAs shell, $N_A = 1.1 \times 10^{18}$ cm^{-3}.

Poisson solver in a Silvaco simulation tool in the vicinity of the p-i-n junction. The bandgap of the InGaP and its offsets to the GaAs depend on the composition and the degree of ordering in the InGaP shell.[29,30] In lattice-matched InGaP, layers grown at 650 °C on GaAs, a type-two heterojunction with a conduction-band discontinuity of $\Delta W_C = -0.1$ eV has been observed.[30] Interface states and strain in between the core and the different shells were not considered. The conduction-band discontinuity of $\Delta W_C = -0.1$ eV forms a negligibly small barrier for electrons generated in the InGaP or p-GaAs layer. On the contrary, holes generated in the n$^+$-GaAs layer are not able to overcome the huge valence-band discontinuity of about $\Delta W_L = +0.5$ eV[29] and are not able to reach the p-contact and contribute to the effective photogenerated charge. The calculated band diagram for the unbiased case further shows that a charge-separating field is present in the intermediate InGaP layer, as well as at the InGaP to p$^+$GaAs junction. Since the outer p-GaAs layer had

Figure 6. a) Schematic drawing of the measurement setup. b) SPCM mapping superimposed on an SEM microscopy image of the fabricated core-multishell p-i-n diode (scale bar is 2 μm). A generated photocurrent is only observable in the unetched nanowire region.

To determine the solar-conversion efficiency of the fabricated nanowire photovoltaic devices, I–V measurements under standard AM 1.5G conditions, provided by a solar simulator operating with a 100 mW cm^{-2} (1 sun) illumination intensity, were carried out (red curves of Figure 7a). A short-circuit current of 479 pA and an open-circuit voltage of 0.5 V were obtained, yielding a fill factor of 52% under 1-sun conditions. This relatively poor fill factor can be attributed to the large series resistance of the device ($R_S \approx 300$ κΩ). The solar-conversion efficiency was determined using the following equation:

$$\eta = V_{oc} \cdot I_{sc} \cdot FF / P_{in} \tag{3}$$

P_{in} was calculated from the product of the illumination power density and the absorption area of the nanowire device. When the maximal projected absorption area – as measured from the SEM images – was used for the calculation, an efficiency of 4.7% was obtained. The achieved performance is similar to that reported for radial homoepitaxial GaAs p-i-n structures,[19] which is among the highest reported efficiencies for III-V-nanowire-based solar cells.[31]

In addition, the photovoltaic properties of the fabricated p-i-n diodes were investigated under high-intensity illumination. For this reason, the laser spot was expanded to 20 μm, now covering the whole nanowire device with a homogenous laser illumination ($\lambda = 532$ nm). Power-dependent photocurrent measurements demonstrated a linear scaling of the photocurrent with illumination intensity (cf., Figure 7c). The photocurrent directly followed the increasing photoexcitation with 0.22 A W^{-1}, with respect to the absorbed illumination power up to an illumination density of at least 150 W cm^{-2}. Thus, the photosensitivity of the nanowire diode remained constant with increasing photoexcitation, making these structures interesting for energy conversion under concentrated illumination. In contrast, the fill factor continuously decreased from 52% to 42% (Figure 7d, blue curve) with increasing illumination power, which might be attributed to sample heating and less-effective cooling, due to the core-multishell approach. Moreover, the voltage drop caused by the series resistance of the p-GaAs shell decreased the voltage applied to the intrinsic p-i-n junction, especially at higher device-current/illumination power. Figure 7d (black curve) shows that the open-circuit voltage was slightly increased and saturated at a level of approximately 1 V for an illumination power above 100 μW. Since this value is larger than $V_{oc} = 0.5$ V, measured under 1-sun conditions, it can be concluded that 1 V represents the upper V_{oc} limit of the fabricated p-i-n nanowire diode. Recombination of carriers might occur in the p-i-n junction at defects present at the core-shell and shell-shell interfaces, and at the surface states. LaPierre et al. reported that these mechanisms drastically decrease the maximum possible V_{oc}.[32] Therefore, the reduction of interface defects and surface passivation should play a major role in the further improvement of core-multishell-nanowire photovoltaic devices.

a thickness of 90 nm, most of the incident light will have been absorbed here. The generated carriers will partly recombine, but also be separated by the internal field. Hence, some of the electrons can easily reach the n-GaAs core, while the generated holes have a short path to the p-contact. The remaining transmitted light will be absorbed by the intermediate InGaP shell, or even by the n-GaAs core, and thus further contribute to the generated photocurrent. It is evident that the described structure is not ideal in terms of ultra-high solar-cell efficiencies. Nevertheless, a reasonable charge separation yielding a photovoltaic effect should be possible under these conditions.

To prove this assumption, we performed scanning-photocurrent-microscopy (SPCM) measurements on the radial nanowire diodes (schematics shown in **Figure 6**a). For this purpose, a tightly focused laser spot ($\lambda = 532$ nm; laser intensity = 300 W cm^{-2}) with a diameter of ≈1.2 μm was raster scanned over the surface of the contacted nanowire (grid step = 200 nm) while the photocurrent was recorded as a function of the illumination position. Figure 6b shows an SPCM map of the investigated device superimposed on an SEM micrograph. The map clearly shows that the region of high photocurrent was located in the unetched p-i-n diode part, where charge separation through the built-in field takes place. Moreover, the photocurrent generation in the nanowire part beyond the p-contact demonstrates that the built-in field was present in the whole nanowire p-i-n junction, which sustains a contacting process. The response was not homogeneous along the wire, but was strongest in the vicinity of the p-contact, in agreement with the smallest series resistance stemming from the p-GaAs shell. On the contrary, no photocurrent was measured in the etched n-GaAs core region, yielding additional proof of the successful removal of the outer shells. Based on the SPCM mapping, the maximal absorption area of the device corresponds to the unetched diode region projected on the substrate surface. This area was calculated as the product of the unetched region length (8 μm) and the physical nanowire diameter (317 nm), both derived from the SEM images.

The black I–V curves given in **Figure 7**a were measured in the dark and prove the high rectification ratio (≈3500 at ±1V) of the fabricated p-i-n diode with leakage currents in the pA range. The ideality factor was estimated as $n = 2.2$ in the low-voltage range (0.2 V < V_{bias} < 0.6 V), from:

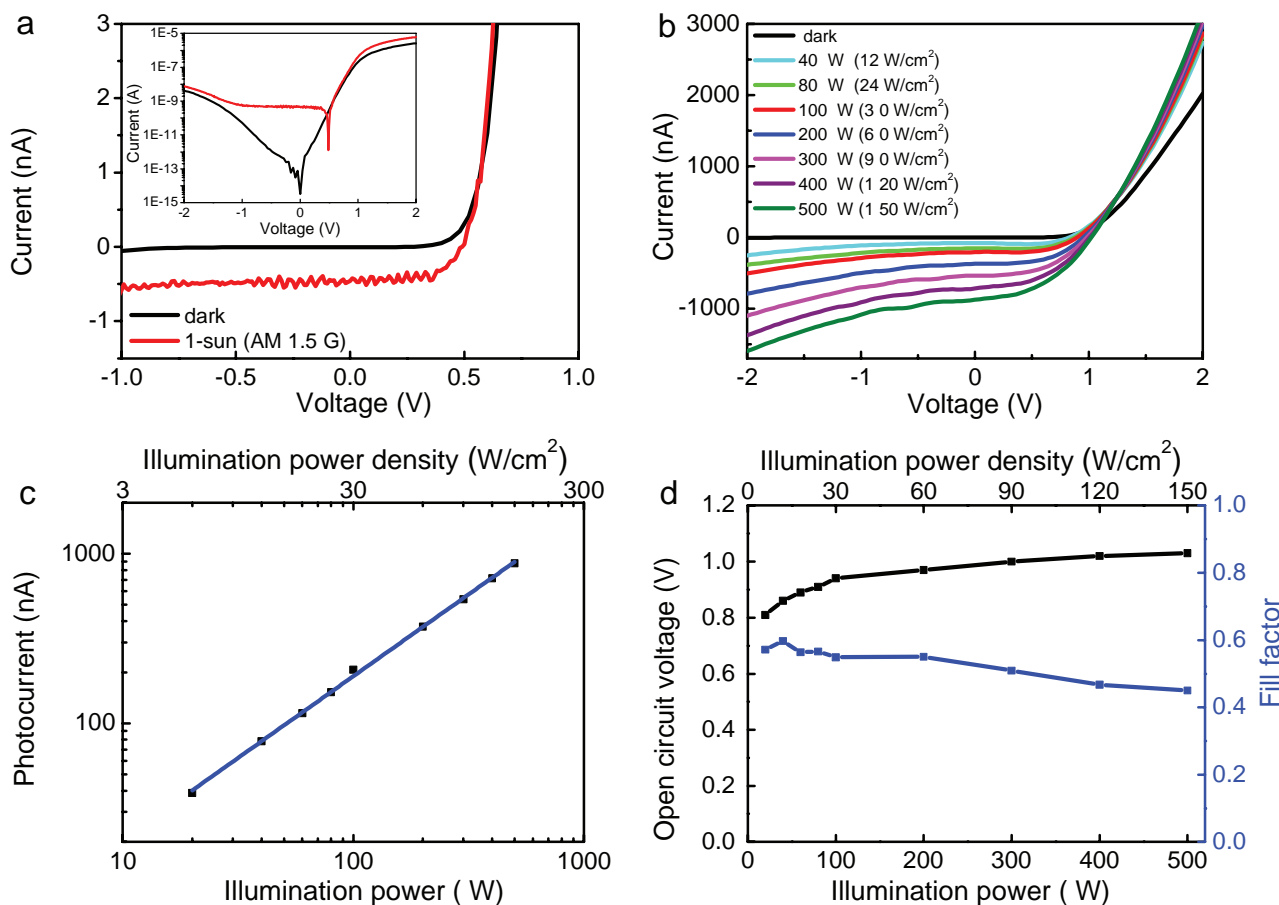$$I = I_0 \cdot \exp\left(\frac{q \cdot V_{bias}}{n \cdot k \cdot T}\right) \tag{2}$$

Figure 7. a) *I–V* characteristics of the p-i-n diode measured without illumination (black) and under 1-sun homogenous illumination (red). The inset shows a semilogarithmic plot. b) The *I–V* characteristics measured under monochromatic homogeneous laser illumination (λ = 532 nm) for various illumination power densities from a defocused laser spot. c) The photocurrent as a function of illumination power. A linear scaling is visible. d) The power dependence of the open-circuit voltage and the fill factor, both measured under monochromatic homogeneous laser illumination (λ = 532 nm) from a defocused laser spot.

3. Conclusions

In summary, a detailed analysis of n-GaAs/InGaP/p-GaAs core-multishell nanowires is presented. CBr_4 enables heavily doped VS-grown p-type GaAs shells with a homogeneous carrier concentration of 1.1×10^{18} cm^{-3} to be produced. Combined with a VLS-grown n-type GaAs nanowire core and an intermediate InGaP shell, we have synthesized a p-i-n diode structure that allows selective chemical etching of the individual shells and, therefore, a simplified contacting process. Electrical characterization proved diode behavior with low reverse currents and high rectification ratios. SEM micrographs revealed a growth-temperature-related transition from {112} side facets for the nanowire core into {110} facets for the outer shells. The pronounced electroluminescence measured at room temperature constitutes the optical quality of the fabricated p-i-n diode. The photovoltaic properties of a single device were determined using spatially resolved and power-dependent photocurrent measurements. A 2D photocurrent mapping demonstrated that charge separation was only observable in the unetched nanowire region. Under homogeneous high-intensity monochromatic illumination (λ = 532 nm), linear scaling of the photocurrent with illumination

intensity, up to an illumination density of at least 150 W cm^{-2}, was presented, which proves the potential for applications in concentrator solar cells. The solar-conversion efficiency was investigated by performing measurements under standard 1-sun AM 1.5G conditions, yielding a short-circuit current of 479 pA, an open-circuit voltage of 0.5 V and a fill factor of 52%. Finally, using these values, an energy-conversion efficiency of 4.7% was obtained, which is among the best data reported for III-V-nanowire-based photovoltaic devices. Further improvement can be expected by optimization of the device structure, including the doping levels and the geometry, optimization of the core-shell and shell-shell interfaces and passivation of surface states.

4. Experimental Section

Growth: The two types of nanowires were grown on GaAs (111) B substrates via Au-catalyzed low-pressure (50 mbar) MOVPE in a commercial AIX200 RF system with a fully non-gaseous source configuration. Trimethylgallium (TMGa), trimethylindium (TMIn), tertiarybutylarsine (TBAs), tertiarybutylphosphine (TBP), tetraethyltin (TESn) and carbontetrabromide (CBr_4) were used as group-III and group-V precursors, as well as n-type and p-type doping precursors,

www.MaterialsViews.com

ADVANCED
FUNCTIONAL
MATERIALS
www.afm-journal.de

FULL PAPER

respectively. The total gas flow of 3.3 L min^{-1} within the reactor was provided by N$_2$ carrier gas, while H$_2$ was used as the source gas.

Prior to growth, monodisperse Au nanoparticles with a diameter of 100 nm, taken from a colloidal solution, were deposited randomly on the substrate. The samples were then transferred to the MOVPE reactor followed by an annealing step at 600 °C for 5 min under TBAs supply with molar fraction of $\chi_{TBAs} = 6.2 \times 10^{-4}$.

The **Type A** nanowires consisted of a nid-i-GaAs core surrounded by a p-GaAs shell (cf., schematic drawing in Figure 1). The nanowire core was grown using TMGa ($\chi_{TMGa} = 1.32 \times 10^{-4}$) and TBAs ($\chi_{TBAs} = 3.16 \times 10^{-4}$) precursors in a two-temperature growth procedure.[33] After the growth started, initiated at 450 °C for 3 min, the growth temperature was adjusted to 400 °C, and the rest of the nanowire was grown. At this lower temperature, additional layer growth on the nanowire side facets was almost completely suppressed and the Au-assisted VLS growth dominated. After 78 min the growth temperature was ramped up to 650 °C and the TBAs mole fraction was increased to $\chi_{TBAs} = 1.1 \times 10^{-3}$ to promote VS shell growth. For a p-type doping of the GaAs shell, CBr$_4$ ($\chi_{CBr4} = 2.6 \times 10^{-5}$) was supplied additionally to the reactor.

The **Type-B** nanowires consisted of an n-GaAs core surrounded by a nid-InGaP and a p-GaAs shell (cf., schematic drawing in Figure 1). These core-multishell nanowires were synthesized as follows: the nanowire core was grown in the earlier-described two-temperature procedure. TESn ($\chi_{TESn} = 1.05 \times 10^{-5}$) was used as an n-type dopant and the supply was started 4 min before nanowire growth was initiated to presaturate the growth seeds with tin. Following a previously described analysis,[34] these conditions yielded a mean carrier concentration of $N_D = 4 \times 10^{18}$ cm^{-3}. After 126 min, the temperature was increased to 650 °C, where the kinetic hindrance of the side-facet growth was overcome and the InGaP shell could be deposited.[6] For this purpose, the group-V precursor was switched from TBAs to TBP ($\chi_{TBP} = 3.1 \times 10^{-3}$), whereas TMGa ($\chi_{TMGa} = 6.28 \times 10^{-5}$) and TMIn ($\chi_{TMIn} = 6.52 \times 10^{-5}$) served as group-III precursors. The ratio χ_{TMIn}/χ_{TMGa} was calibrated beforehand via EDS measurements to produce shells with the composition of In$_{0.5}$Ga$_{0.5}$P, lattice-matched to the GaAs core. After 20 s, the precursors TMIn and TBP were switched off and p-GaAs shells were grown for 3 min with the parameters described above. These growth parameters resulted in shell thicknesses of $r_{InGaP} \approx 20$ nm and $r_{p-GaAs} \approx 90$ nm.

Electron Microscopy: Characterization of the nanowire-shell growth and the etching process was performed via SEM (LEO 1530), while EDS was carried out in a high-resolution TEM (*HR-TEM*) (Philips Tecnai F20). The TEM samples were prepared by a dry-transfer of the nanowires onto a Cu-grid coated with a thin film of holey carbon. This was done by simple physical contact of the TEM grid to the substrate with free-standing nanowires.

Optoelectrical Characterization: For the optoelectronic characterization the structures were deposited on special prepatterned insulating carriers and finally contacted by the electron-beam lithography (E-Beam) and evaporation technique. Pt (5 nm)/Ti (10 nm)/Pt (10 nm)/Au (400 nm) annealed at 360 °C for 30 s was used as an ohmic contact to the p-GaAs area, while Pd (50 nm)/Ge (170 nm)/Au (80 nm) annealed for 30 s at 280 °C formed ohmic contacts with the n-GaAs nanowire core.[35] In addition, top-gated MISFET devices with about 30 nm SiN$_x$ gate dielectric and Ti/Au gate metal were fabricated on i-GaAs/p-GaAs core-shell nanowires to verify the type of conductivity.

Electrical measurements were carried out using a Keithley SCS 4200 current–voltage analyzer. Electroluminescence (EL) as well as spatially resolved and power-dependent photocurrent measurements were performed at room temperature in an optical cryostat fitted with an XY piezo-driven scanning stage. An optical excitation for the photocurrent measurements was made using a continuous-wave (CW) Nd:YVO$_4$ laser with $\lambda = 532$ nm, focused by a 50× microscope objective lens. For the EL measurements, the signals were collected using the same objective lens and were focused onto the entrance slit of a 500 mm Czerny–Turner monochromator equipped with a 150 mm^{-1} grating. The spectrally dispersed signal was detected using a liquid-nitrogen (LN$_2$)-cooled charge-coupled device. The solar-conversion efficiency was determined under standard AM 1.5G conditions provided by a Voss Electronic solar simulator. All of the optoelectronic measurements presented in this work were carried out on the same nanowire device, which had a diameter of 317 nm.

Supporting Information

Supporting Information is available from the Wiley Online Library or from the author.

Acknowledgements

[1] P. Yang, R. Yan, M. Fardy, *Nano Lett.* **2010**, *10*, 1529.

[2] L. J. Lauhon, M. S. Gudiksen, D. Wang, C. M. Lieber, *Nature* **2002**, *420*, 57.

[3] F. Qian, S. Gradecak, Y. Li, C.-Y. Wen, C. M. Lieber, *Nano Lett.* **2005**, *5*, 2287.

[4] B. Tian, X. Zheng, T. J. Kempa, Y. Fang, N. Yu, G. Yu, J. Huang, C. M. Lieber, *Nature* **2007**, *449*, 885.

[5] J. Kupec, R. L. Stoop, B. Witzigmann, *Opt. Express* **2010**, *18*, 27589.

[6] N. Sköld, L. S. Karlsson, M. W. Larsson, M.-E. Pistol, W. Seifert, J. Trägardh, Lars Samuelson, *Nano Lett.* **2005**, *5*, 1943.

[7] P. Parkinson, H. J. Joyce, Q. Gao, H. H. Tan, X. Zhang, J. Zou, C. Jagadish, L. M. Herz, M. B. Johnston, *Nano Lett.* **2009**, *9*, 3349.

[8] B. Hua, J. Motohisa, Y. Kobayashi, S. Hara, T. Fukui, *Nano Lett.* **2009**, *9*, 112.

[9] R. Chen, T.-T. D. Tran, K. W. Ng, W. S. Ko, L. C. Chuang, F. G. Sedgwick, C. Chang-Hasnain, *Nature Photonics* **2011**, *5*, 170.

[10] C. P. T. Svensson, T. Martensson, J. Trägardh, C. Larsson, M. Rask, D. Hessman, Lars Samuelson, J. Ohlsson, *Nanotechnology* **2008**, *19*, 305201.

[11] K. Tomioka, J. Motohisa, S. Hara, K. Hiruma, T. Fukui, *Nano Lett.* **2010**, *10*, 1639.

[12] L. C. Chuang, F. G. Sedgwick, R. Chen, W. S. Ko, M. Moewe, K. W. Ng, T.-T. D. Tran, C. Chang-Hasnain, *Nano Lett.* **2011**, *11*, 385.

[13] E. C. Garnett, M. L. Brongersma, Y. Cui, M. D. McGehee, *Annu. Rev. Mater. Res.* **2011**, *41*, 269.

[14] O. L. Muskens, J. Gómez Rivas, R. E. Algra, E. P. A. M. Bakkers, Ad. Lagendijk, *Nano Lett.* **2008**, *8*, 2638.

[15] L. Cao, J. S. White, J.-S. Park, J. A. Schuller, B. M. Clemens, M. L. Brongersma, *Nat. Mater.* **2009**, *8*, 643.

[16] E. Garnett, P. Yang, *Nano Lett.* **2010**, *10*, 1082.

[17] A. Gu, Y. Huo, S. Hu, T. Sarmiento, E. Pickett, D. Liang, S. Li, A. Lin, S. Thombare, Z. Yu, S. Fan, P. McIntyre, Y. Cui, J. Harris, *35th IEEE Photovoltaics Specialists Conf., 2010* **2010**, 002034.

[18] B. M. Kayes, H. A. Atwater, N. S. Lewis, *J. Appl. Phys.* **2005**, *97*, 114302.

[19] C. Colombo, M. Heiß, M. Grätzel, A. Fontcuberta i Morral, *Appl. Phys. Lett.* **2009**, *94*, 173108.

[20] J. A. Czaban, D. A. Thompson, R. R. LaPierre, *Nano Lett.* **2009**, *9*, 148.

[21] G. Mariani, P.-S. Wong, A. M. Katzenmeyer, F. Leonard, J. Shapiro, Diana L. Huffaker, *Nano Lett.* **2011**, *11*, 2490.

[22] C. Gutsche, I. Regolin, K. Blekker, A. Lysov, W. Prost, F. J. Tegude, *J. Appl. Phys.* **2009**, *105*, 024305.

[23] T. F. Kuech, M. A. Tischler, P.-J. Wang, G. Scilla, R. Potemski, F. Cardone, *Appl. Phys. Lett.* **1988**, *53*, 1317.

[24] M. C. Hanna, Z. H. Lu, A. Majerfeld, *Appl. Phys. Lett.* **1991**, *58*, 164.

[25] N. Sköld, J. B. Wagner, G. Karlsson, T. Hernán, W. Seifert, M.-E. Pistol, L. Samuelson, *Nano Lett.* **2006**, *6*, 2743.

[26] G. Zhang, K. Tateno, T. Sogawa, H. Nakano, *Appl. Phys. Express* **2008**, *1*, 064003.

[27] T. Kobayashi, K Taira, F. Nakamura, H. Kawai, *J. Appl. Phys.* **1989**, *65*, 4898.

[28] J. W. Lee, S. J. Pearton, C. R. Abernathy, W. S. Hobson, F. Ren, C. S. Wu, *Solid-State Electron.* **1995**, *38*, 1871.

[29] G. S. Horner, A. Mascarenhas, R. G. Alonso, D. J. Friedman, K. Sinha, K. A. Bertness, J. G. Zhu, J. M. Olson, *Phys. Rev. B: Condens. Matter* **1993**, *48*, 4944.

[30] Q. Liu, S. Derksen, W. Prost, A. Lindner, F. J. Tegude, *J Appl. Phys.* **1996**, *79*, 305.

[31] K. Sun, A. Kargar, N. Park, K. N. Madsen, P. W. Naughton, T. Bright, Y. Jing, D. Wang, *IEEE J. Selected Topics Quantum Electron.* **2011**, *17*, 1033.

[32] R. R. LaPierre, *J. Appl. Phys.* **2011**, *109*, 034311.

[33] H. J. Joyce, Q. Gao, H. H. Tan, C. Jagadish, Y. Kim, X. Zhang, Y. Guo, J. Zou, *Nano Lett.* **2007**, *7*, 921.

[34] C. Gutsche, A. Lysov, I. Regolin, K. Blekker, W. Prost, F.-J. Tegude, *Nanoscale Res. Lett.* **2011**, *6*, 65.

[35] C. Gutsche, A. Lysov, I. Regolin, A. Brodt, L. Liborius, J. Frohleiks, W. Prost, F.-J. Tegude, *J. Appl. Phys.* **2011**, *110*, 014305.